

# Six-Dimensional Cooling Simulations for the Muon Collider

Pavel Snopok and Gail Hanson

Department of Physics and Astronomy, University of California Riverside, Riverside, CA 92521, USA

The two cooling channels based on the RFOFO ring concept are considered and simulated. One of them is the RFOFO helix, also known as the Guggenheim. The helical shape of the channel resolves the injection and extraction issues as well as the absorber overheating issue. The issue of the RF breakdown in the magnetic field is addressed in the so-called open cavity cooling channel lattice with magnetic coils in the irises of the RF cavities. The details of the tracking studies of both channels are presented and compared to the performance of the original RFOFO cooling ring design.

## 1. RFOFO Cooling Ring

In a Muon Collider design the muon beam 6D phase space volume must be reduced several orders of magnitude in order to be able to further accelerate it. Ionization cooling is currently the only feasible option for cooling the beam within the muon lifetime ( $\tau_0 = 2.19 \mu s$ ). The RFOFO ring Palmer et al. [2005], Berg et al. [2003] is one of the feasible options currently under active investigation along with other designs Kaplan [2007], Alexahin et al. [2007], Johnstone et al. [2005]. The RFOFO ring provides a significant reduction in the six-dimensional emittance in a small number of turns with a relatively low particle loss factor. 6D cooling is achieved by employing the concept of emittance exchange. When a dispersive beam passes through a wedge absorber in such a way that higher momentum particles pass through more material, both the longitudinal and the transverse emittances are reduced. However, the design of the injection and extraction channels and kickers is very challenging for the RFOFO, and the ring could not be used as is, because the bunch train is too long to fit in the ring. Both problems would be removed in the RFOFO helix, also known as the Guggenheim channel Snopok et al. [2009]. In addition, using the helix solves another important issue, namely, the overheating in the absorbers.

The main parameters of the original RFOFO design are summarized in Table I and compared to the parameters of the Guggenheim channel. The layout of the RFOFO ring is shown in Fig. 1. The results of particle tracking through the RFOFO channel in the code G4Beamline Roberts are used as the point of reference while comparing the RFOFO and Guggenheim channel efficiencies.

## 2. Guggenheim Helix

The layout of the Guggenheim channel to a large extent repeats the one of the RFOFO ring, except for the three meters of separation between the layers of the helix. As a result, the circumference of the helix

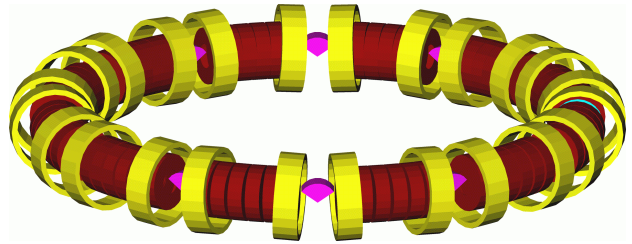


Figure 1: RFOFO ring layout. Yellow—tilted magnetic coils with alternating currents to provide necessary bending and focusing, and generate dispersion, purple—wedge absorbers for cooling and emittance exchange, brown—RF cavities for restoring the longitudinal component of the momentum.

		RFOFO	Guggenheim
RF frequency	[MHz]	201.25	201.25
RF gradient	[MV/m]	12.835	12.621
Maximum axial field	[T]	2.77	2.80
Pitch	[m]	0.00	3.00
Pitch angle	[deg]	0.00	5.22
Circumference	[m]	33.00	32.86
Radius	[m]	5.252	5.230
Coil tilt (wrt orbit)	[deg]	3.04	3.04
Average momentum	[MeV/c]	220	220
Reference momentum	[MeV/c]	201	201
Absorber angle	[deg]	110	110
Absorber vertical offset	[cm]	9.5	9.5
Absorber axial length	[cm]	27.13	27.13

Table I Parameters of the RFOFO ring compared to the Guggenheim helix.

has to be slightly smaller than that of the ring to keep the arclength of one revolution intact.

Figure 2 shows the 5-turn layout which has been simulated. Along with the unshielded case with all the magnetic coils of all layers contributing to the magnetic field guiding muons, another scheme has been considered, with shielding between individual layers. Both layouts include safety windows around absorbers and Be windows in the RF cavities.

The simulation details can be found in Snopok et al. [2009]. Here we show only the six-dimensional emit-

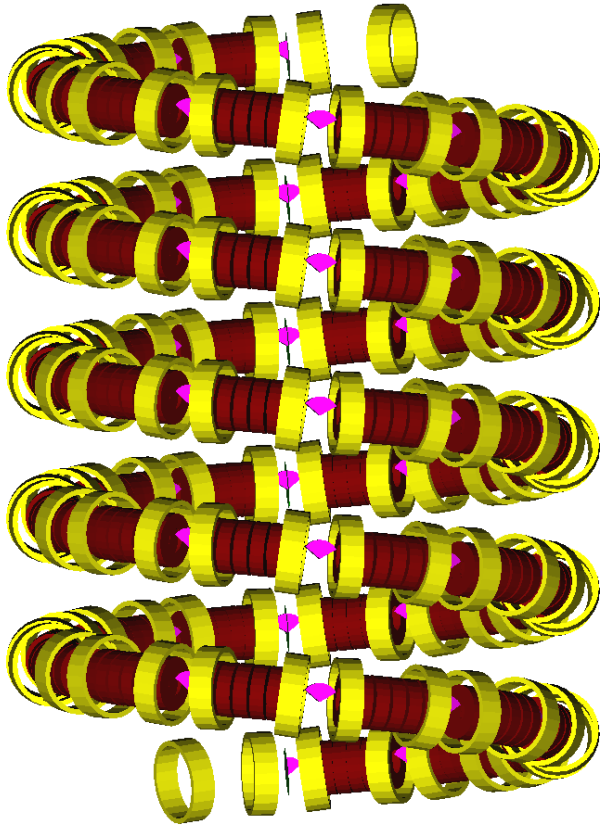


Figure 2: Multilayer Guggenheim channel layout. Color-coding is the same as for Fig. 1.

tance reduction (see Fig. 3), and the transmission (see Fig. 4) as functions of the number of turns. The transmission is measured as the ratio of the number of particles at a certain arclength to the initial number of particles. The muon decay and stochastic processes are taken into account. The solid line is used for the RFOFO ring, which serves as a reference, the dashed line is the Guggenheim channel with shielding between layers and no windows in absorbers or RF cavities (the idealized Guggenheim, the performance of which should not differ significantly from the RFOFO ring, which is indeed the case), and the dash-dotted line is for the realistic Guggenheim with shielding between layers and windows in both absorbers and RF cavities.

Figure 3 clearly demonstrates significant six-dimensional cooling; however, the performance of the cooling channel is seriously affected by the use of absorber and RF windows. These results are in agreement with earlier studies for the RFOFO ring Palmer et al. [2005].

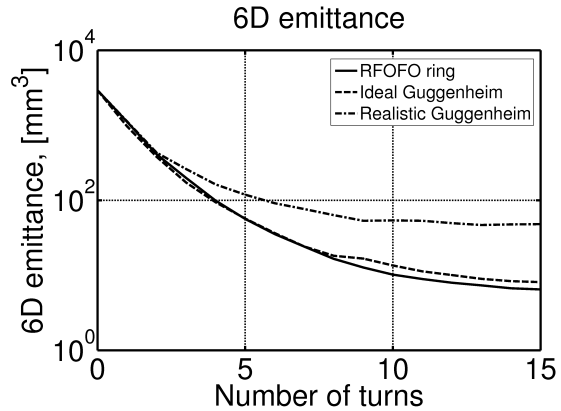


Figure 3: Six-dimensional emittance reduction vs number of turns.

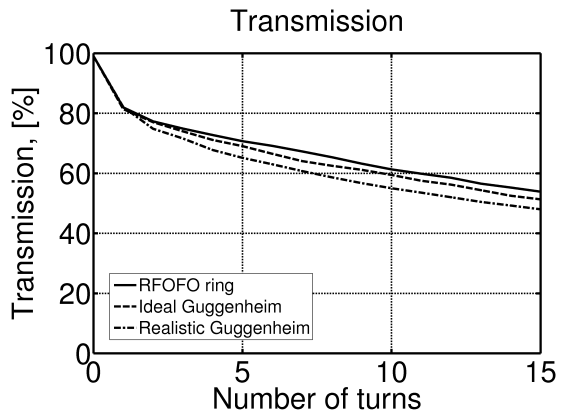


Figure 4: Transmission—percent of surviving muons vs number of turns.

### 3. RF Breakdown and the Open Cavity Lattice

Various studies suggest that the presence of the magnetic field disrupts the performance of RF cavities by causing breakdown Norem et al. [2008], Palmer et al. [2008]. Thus, it was proposed to consider an alternative layout of the cooling channel, the so-called open cavity lattice Palmer et al. [2009a]. The concept itself consists of two parts: a) moving the solenoidal coils from over the RF cavities into the irises; and b) shaping the RF cavities such that the walls of the cavities are predominantly parallel to the magnetic field lines (see Fig. 5), which hopefully solves the problem of the breakdown. Current layout illustrated in Figure 6 does not include specifically shaped RF cavities; instead a simplified pillbox geometry is used.

The main parameters of the open cavity lattice are summarized in Table II and compared to the parameters of the original RFOFO channel.

The new cooling ring has 12 cells with three RF

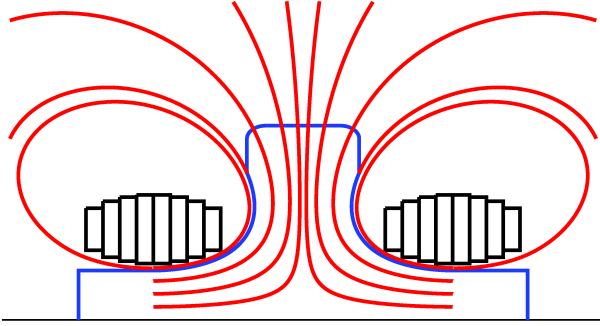


Figure 5: Open cavity shape. Black—coils generating the magnetic field, blue—walls of the RF cavity, red—magnetic field lines.

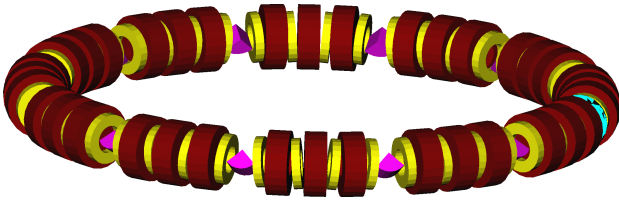


Figure 6: Open cavity layout, color-coding is the same as for Fig. 1.

cavities in each and four solenoidal coils in the irises. These coils bear currents with the following densities:  $63 \text{ A/mm}^2$ ,  $45 \text{ A/mm}^2$ ,  $-45 \text{ A/mm}^2$ ,  $-63 \text{ A/mm}^2$ .

The circumference of the ring is 30.72 meters. The idea of tipping the solenoids, similar to the RFOFO ring concept, is employed in this layout to generate an average vertical magnetic field of 0.136 T providing necessary bending. Solenoid axes are tilted  $4.9^\circ$  above or below the orbital midplane depending on the direction of the current. The centers of the solenoids are displaced radially outward from the reference circle by 21 mm to minimize the integrated on-axis radial field, thus, vertical beam deviations. This technique allows to save 2% of the beam that would be lost with

		Open cavity	RFOFO
RF frequency	[MHz]	201.25	201.25
RF gradient	[MV/m]	16.075	12.835
Maximum axial field	[T]	3.23	2.80
Circumference	[m]	30.72	33.00
Radius	[m]	4.889	5.252
Reference momentum	[MeV/c]	214	201
Coil tilt	[deg]	4.90	3.04
Current densities	[A/mm <sup>2</sup> ]	[63, 45, -45, -63]	[95, -95]
Absorber angle	[deg]	90	110
Absorber vertical offset	[cm]	12.0	9.5
Absorber axial length	[cm]	24.00	27.13

Table II Parameters of the open cavity lattice compared to the RFOFO ring lattice.

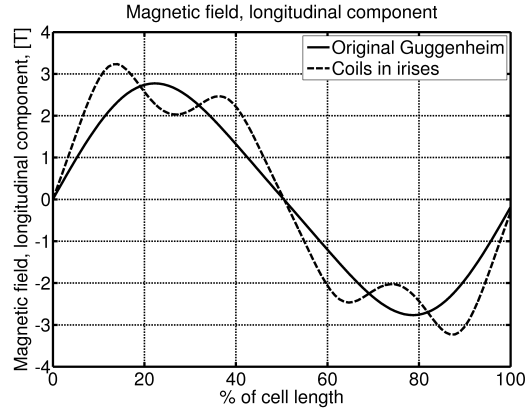


Figure 7: Longitudinal field component. Solid line—original RFOFO ring or Guggenheim helix lattice, dashed line—open cavity lattice.

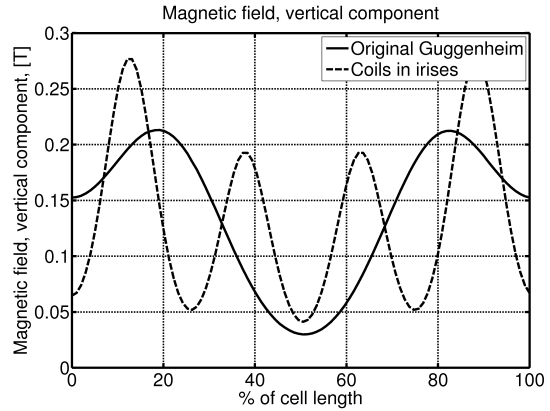


Figure 8: Vertical field component. Solid line—original RFOFO ring or Guggenheim helix lattice, dashed line—open cavity lattice.

no offset.

The fact that the solenoids are tilted leads to the reduction of the amount of space available for the RF system; hence, the energy gain per cell is limited, which, in turn, limits the angle of the wedge absorber to approximately  $90^\circ$  (compared to  $110^\circ$  in RFOFO).

Figures 7–9 illustrate the difference between field components for the original RFOFO design and the new design with coils in irises. Since there are four coils per cell, all field profiles have more complicated shapes; however, the overall magnitudes are similar.

The peak in the longitudinal field is still approximately 3 T; the radial component is more pronounced, but still small compared to both the vertical and the longitudinal components. The vertical component is everywhere positive providing an average bending field of 0.136 T.

Deviation of the closed orbit along one periodic cell for various momenta ranging from 150 MeV/c to 250

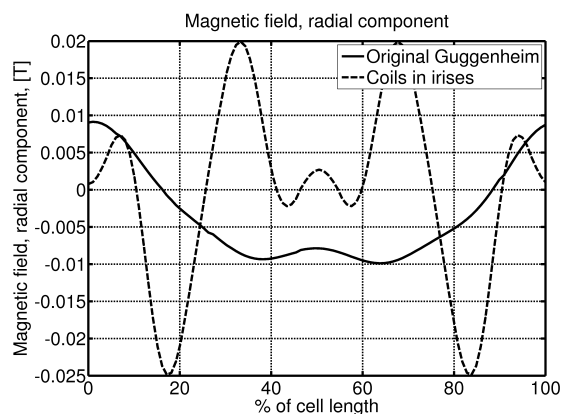


Figure 9: Radial field component. Solid line—original RFOFO ring or Guggenheim helix lattice, dashed line—open cavity lattice.

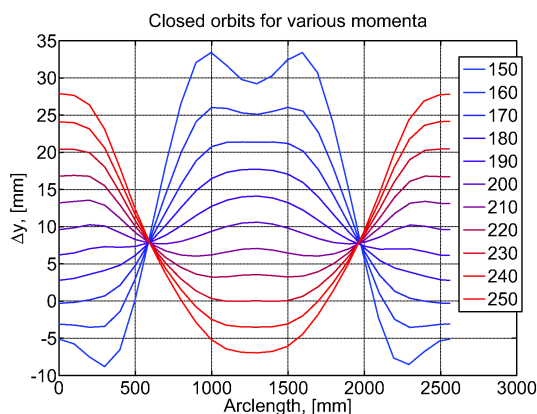


Figure 11: Closed orbit vertical offset along one cell of the cooling channel (2560 mm) for various momenta from 150 MeV/c to 250 MeV/c.

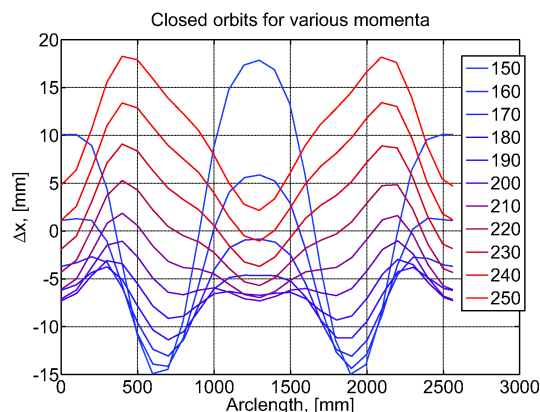


Figure 10: Closed orbit horizontal offset along one cell of the cooling channel (2560 mm) for various momenta from 150 MeV/c to 250 MeV/c.

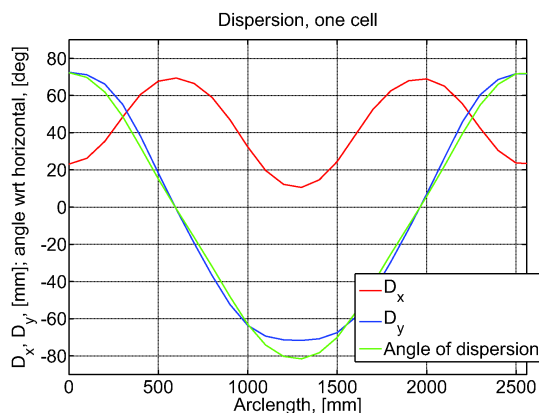


Figure 12: Dispersion plot. Red line—horizontal, blue line—vertical, green—orientation of dispersion with respect to the horizontal axis.

MeV/c are shown in Fig. 10–11.

The dispersion calculation (Fig. 12) shows that the dispersion at the absorber plane (beginning of the cell) is primarily in the vertical direction, at an angle of  $\sim 20^\circ$  from the vertical axis. This fact suggests the orientation of the absorbers. The dispersion in the center of the cell is negative, again mainly in the vertical direction.

Closed orbit deviation for different momenta ranging from 150

### 3.1. Dynamics of particles in the open cavity lattice

In this section we compare the performance of the open cavity lattice with that of the RFOFO ring discussed in Section 1. Figures 13–16 illustrate the change in the longitudinal, transverse and six-dimensional emittance versus the number of turns for

both the open cavity lattice and the RFOFO ring with all the decay and stochastic processes taken into account. As one can see from these tracking results, the open cavity lattice clearly performs very similar to the RFOFO lattice, sometimes even slightly better for the same initial beam. The open cavity ring is slightly smaller than the RFOFO ring: 30.72 m in circumference vs 33.00 m, correspondingly. However, there is less room for RF cavities in the open cavity layout, hence, higher gradients are required (as can be seen from Table II).

The cooling effect in both transverse and longitudinal directions is evident from Fig. 17–19.

An alternative approach to using the open cavity or any other type of magnetically insulating lattice is to research the techniques allowing RF cavities withstand more magnetic field without breaking down. Such techniques include atomic layer deposition creating a thin layer of material on the cavity walls Norem

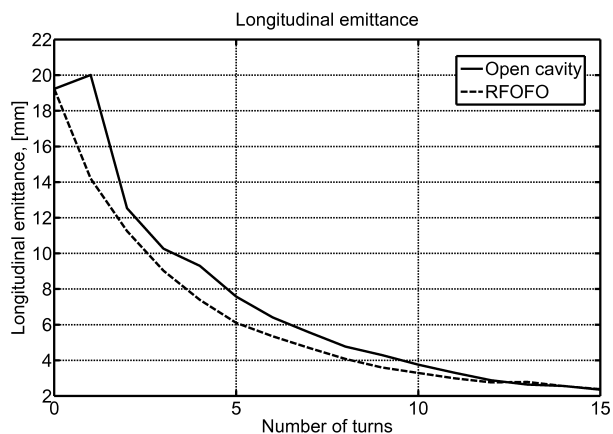


Figure 13: Longitudinal emittance reduction vs number of turns. Solid line—open cavity lattice, dashed line—RFOFO.

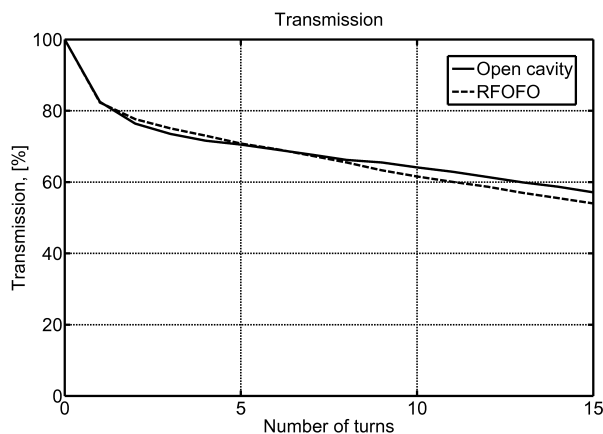


Figure 16: Transmission—percent of surviving muons vs number of turns. Solid line—open cavity lattice, dashed line—RFOFO.

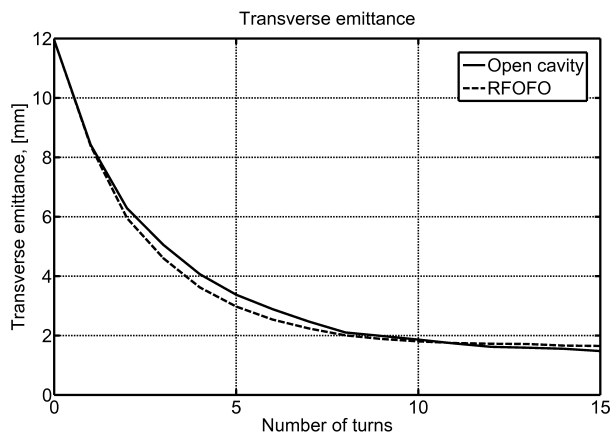


Figure 14: Transverse emittance reduction vs number of turns. Solid line—open cavity lattice, dashed line—RFOFO.

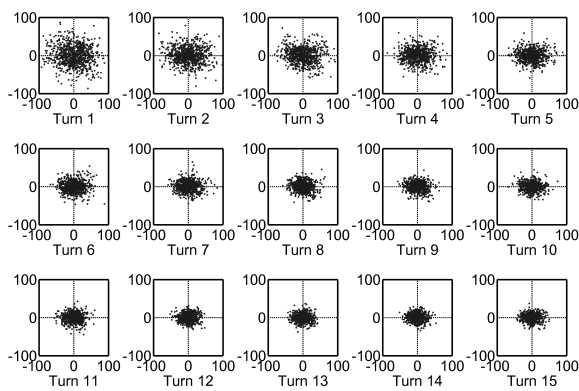


Figure 17: Phase portraits in the  $(x - p_x)$  plane for different number of turns.

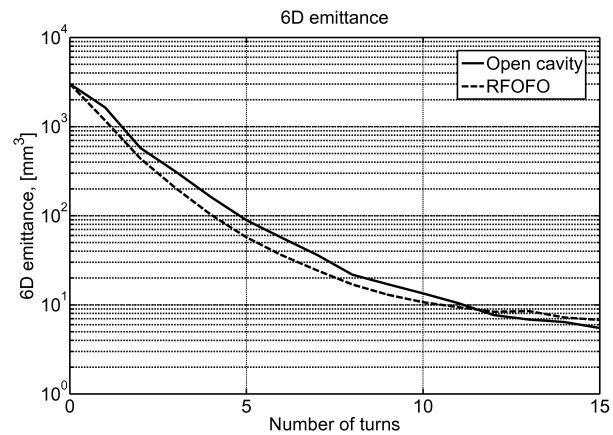


Figure 15: Six-dimensional emittance reduction vs number of turns. Solid line—open cavity lattice, dashed line—RFOFO.

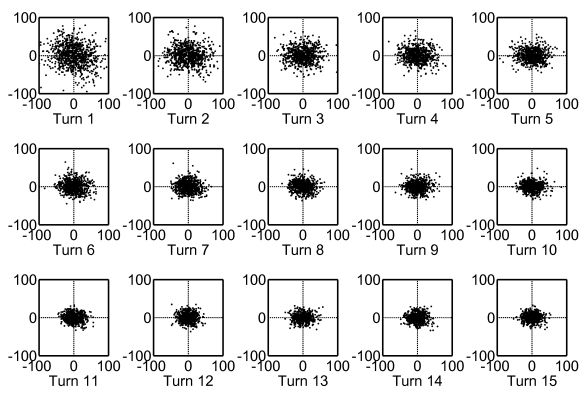


Figure 18: Phase portraits in the  $(y - p_y)$  plane for different number of turns.

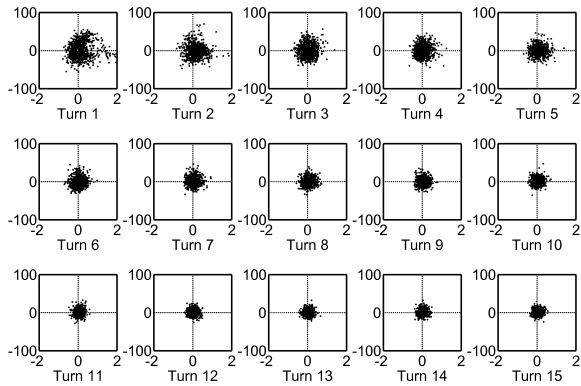


Figure 19: Phase portraits in the  $(t-p_z)$  plane for different number of turns.

et al. [2009], high-pressure gas filled cavities Chung et al. [2009], dielectric-loaded cavities Popovic et al. [2009], and using other materials such as Al or Be and low temperatures Palmer et al. [2009b].

## References

- R. Palmer et al., Phys. Rev. ST Accel. Beams **8**, 061003 (2005).
- J. S. Berg, R. C. Fernow, and R. B. Palmer, Journal of Physics G: Nuclear and Particle Physics **29**, 1657 (2003), doi: 10.1088/0954-3899/29/8/325.
- D. Kaplan (2007), arXiv: 0711.1523v1.
- Y. Alexahin, K. Yonehara, and R. Palmer, in *Proceeding of Particle Accelerator Conference* (2007).
- C. Johnstone, M. Berz, and K. Makino, in *Proceedings of Particle Accelerator Conference* (2005), pp. 3526–3529.
- P. Snopok, G. Hanson, and A. Klier, IJMPA **24(5)**, 987 (2009).
- T. Roberts, *G4Beamline, a “swiss army knife” for Geant4, optimized for simulating beamlines*, <http://www.muonsinc.com>.
- J. Norem et al., Tech. Rep. NFMCC-doc-527-v1, NFMCC (2008).
- R. Palmer et al., Tech. Rep. NFMCC-doc-528-v2, NFMCC (2008).
- R. Palmer et al. (2009a), <http://www.cap.bnl.gov/mumu/conf/MC-090125/talks/RPalmer1-090125.pdf>.
- J. Norem et al., in *Proceeding of Particle Accelerator Conference* (2009).
- M. Chung et al., Tech. Rep. NFMCC-doc-532-v2, NFMCC (2009).
- M. Popovic, A. Moretti, and M. L. Neubauer, in *Proceeding of Particle Accelerator Conference* (2009).
- R. Palmer et al. (2009b), presentation at the MuCool RF Workshop.